Dicer-like 5 deficiency confers temperature-sensitive male sterility in maize

Chong Teng[1†], Han Zhang[2†], Reza Hammond[3], Kun Huang[3], Blake C. Meyers[1,4*], Virginia Walbot[2*]

Affiliations:

[1]Donald Danforth Plant Science Center, 975 N. Warson Rd, St. Louis, MO 63132, USA.

[2]Department of Biology, Stanford University, Stanford, CA 94305, USA.

[3]Delaware Biotechnology Institute, University of Delaware, Newark, DE 19716, USA.

[4]University of Missouri – Columbia, Division of Plant Sciences, 52 Agriculture Lab, Columbia, MO 65211, USA.

[*]**Correspondence to: walbot@stanford.edu (V.W.); bmeyers@danforthcenter.org (B.C.M.)**

[†]These authors contributed equally to this work.

Abstract

Small RNAs play important roles during plant development by regulating transcript levels of target mRNAs, maintaining genome integrity, and reinforcing DNA methylation. *Dicer-like 5* (*Dcl5*) is proposed to be responsible for precise slicing in many monocots to generate diverse 24-nt phased, secondary small interfering RNAs (phasiRNAs), which are exceptionally abundant in meiotic anthers of diverse flowering plants. The importance and functions of these phasiRNAs remain unclear. Here, we characterized several mutants of *dcl5*, including alleles generated by the Clustered Regularly Interspaced Short Palindromic Repeats (CRISPR) *Cas9* system and a transposon-disrupted allele. We report that *dcl5* mutants have few or no 24-nt phasiRNAs, develop short anthers with defective tapetal cells, and exhibit temperature-sensitive male fertility. We propose that DCL5 and 24-nt phasiRNAs are critical for fertility under growth regimes for optimal yield.

Introduction

Three major classes of endogenous small RNAs (sRNAs) exist in plants: microRNAs (miRNAs), heterochromatic small interfering RNAs (hc-siRNAs), and phased, secondary small interfering RNAs (phasiRNAs). From extensive sRNA sequencing in plants, numerous loci generating phasiRNAs have been reported; in grasses, phasiRNAs are enriched in flowers, particularly male reproductive organs [1–5]. In this context, phasiRNA production is initiated by miRNA-mediated cleavage of RNA polymerase II transcripts of two classes of *PHAS* loci. Subsequently, the 3' portion of cleaved transcripts is converted to double-stranded RNA, a substrate for precise chopping

24 by DICER-LIKE 4 (DCL4) yielding 21-nt products; a distinct, proposed role for DCL5 is
25 generation of 24-nt phasiRNAs [3-5]. The 21-nt phasiRNAs are highly abundant during
26 initial cell fate setting in maize anthers [1] and are important for male fertility in rice [6,7].
27 The 24-nt phasiRNAs accumulate coincident with meiotic start, peak during meiosis, and
28 persist at lower levels afterwards; this pattern has generated speculation that they regulate
29 meiosis [8,9].
30
31 In angiosperms, five DICER-LIKE (DCL) proteins have been described and
32 partially characterized [10]. DCL1 is important for miRNA biogenesis, as illustrated by
33 regulation of meristem determinacy in maize inflorescences [11]. In *Arabidopsis thaliana*,
34 DCL2 processes viral- and transgene-derived siRNAs [12]; DCL3 produces 24-nt hc-
35 siRNAs, which then direct DNA methylation of target loci [13]. In many plants including
36 *Oryza sativa* (rice), DCL4 generates 21-nt *trans*-acting siRNAs and phasiRNAs [4].
37 Although the functions of these four *DCL* genes are well conserved in flowering plants,
38 these genes have partially overlapping functions [12,14]. A fifth, more recently described
39 and named gene, *Dcl5*, is monocot-specific [10]. To better understand the function of DCL5
40 and its proposed role in 24-nt phasiRNA biogenesis [1], we characterized maize *dcl5*
41 mutants generated using either a high efficiency CRISPR-mediated gene editing system
42 [15] or transposon-based mutagenesis. Here, we report that *dcl5* mutants have few or no 24-
43 nt phasiRNAs, exhibit defects in tapetal cell differentiation, and show temperature-
44 sensitive male fertility. We propose that DCL5-mediated generation of 24-nt phasiRNAs
45 is required for fertility at temperatures that are optimal for maize yield.
46

47 **Results**

48 **Null mutants of the maize *Dcl5* gene confer male-sterility**

49 Using a CRISPR system targeting the middle of the encoded protein [15], we
50 generated four alleles for analysis (Fig. 1A), and from T_0 plants we developed stable lines
51 that show Mendelian inheritance of *dcl5-1* (Fig. 1B, Supplementary Table 1 and
52 Supplementary Figure 1). *dcl5-1* and *dcl5-4* are frameshift mutants with transcript levels
53 reduced to about a third of their wild type siblings; in contrast, *dcl5-2* (3 bp deletion) and
54 *dcl5-3* (12 bp deletion, 1 bp substitution) have similar or higher transcript levels
55 compared to control siblings (Fig. 1B and Supplementary Figure 2). Wild type and
56 heterozygous *dcl5-1//Dcl5* plants greenhouse-grown at 32° C maximum day/21° C
57 minimum night were identical in whole plant architecture, anther morphology, and
58 fertility. Under the same conditions, homozygous *dcl5-1* plants were male sterile (Fig.
59 1C). Compared to their fertile siblings, sterile *dcl5-1* plants lacked visible differences in
60 tassels and spikelets, however, the sterile anthers were shorter, contained shrunken
61 pollen, and did not exert from the spikelets (Fig. 1C and Supplementary Figure 3).
62 Sporadically, a few anthers exerted and shed viable pollen. Under field conditions, all
63 four alleles showed male sterility and we did not observe any differences in phenotype
64 between alleles. No genomic editing was detected in the homologous sequence in *Dcl3*
65 which is the most likely potentially off-target locus (Supplementary Figure 4). To further,
66 independently verify the observation of male sterility, we acquired an additional allele
67 from the transposon-based Illumina-Mu population [16] (*dcl5-mu03*, line mu-
68 illumina_139042.7). *dcl5-mu03* showed obvious male sterility in both greenhouse and

69 field conditions (Supplementary Figure 5 and Supplementary Table 1). We concluded
70 that *Dcl5* is required for robust male fertility.
71

72 ***dcl5-1* mutants exhibit tapetal defects**

73 To investigate whether *dcl5-1* plants display defects in anther cell patterning, we
74 used confocal microscopy and found normal somatic layer architecture without defects in
75 initial cell differentiation (Supplementary Figure 6). In addition, chromosome pairing,
76 alignment, and meiotic progression were normal in *dcl5-1* meiocytes (Supplementary
77 Figure 7A-L). The *dcl5-mu03* meiocytes also routinely completed meiosis and produced
78 haploid gametophytes (Supplementary Figure 7M, N). Transmission electron microscopy
79 was utilized to visualize nuclei and other cell organelles at higher resolution. During the
80 mid-meiosis stage (2 to 2.5 mm anthers), normal tapetal cells were densely packed with
81 dark-staining materials and were mostly binucleate (Fig. 2A and Supplementary Figure
82 8). In contrast, the tapetal cells in *dcl5-1* were pale and mostly mononucleate, and many
83 cell organelles were not clearly resolved (Fig. 2B and Supplementary Figure 8). Whole
84 mount, fluorescence microscopy was used to quantify binucleate status in *dcl5-1* and
85 fertile anthers. In 1.5 mm anthers (prophase I), there were five-fold fewer binucleated
86 tapetal cells in *dcl5-1*; a significant difference persisted at 2.5 mm (meiosis II) and a large
87 difference remained at 3.0 mm (post-meiosis) (Fig. 2 and Supplementary Figure 9). In
88 extensive confocal microscopic examination of *dcl5-1* anthers, we observed no
89 significant or consistent differences in cell number or volume compared to fertile
90 siblings. About one week after the completion of meiosis (2.5 mm stage), the tapetum
91 starts programmed cell death, vacuolates, collapses, and disappears in the *dcl5-1//Dcl5*

92 anthers (Supplementary Figure 10); in contrast, the tapetum is developmentally delayed
93 and retained in the *dcl5-1* anthers (Supplementary Figure 10). The middle layer in *dcl5-*
94 *1//Dcl5* collapses and disappears, yet it is largely retained in *dcl5-1* (Supplementary
95 Figure 10). Collectively, these observations indicate that tapetal development is delayed
96 or arrested in *dcl5* mutants and that the *dcl5* tapetal cells are therefore likely defective in
97 conducting post-meiotic functions supporting pollen maturation.
98

99 **Tapetum- and meiocyte-specific *Dcl5* expression**

100 To obtain a comprehensive spatiotemporal profile of maize *Dcl5* expression, we
101 queried microarray, published and newly-generated RNA-seq (Supplementary Table 2),
102 and proteomics data. *Dcl5* transcripts are highly enriched in tassels, cobs, embryos, and
103 seeds [17,18], as well as fertile anthers. In contrast, DCL5 protein is low in 1.0 mm, pre-
104 meiotic anthers and extremely high in 2.0 mm mid-meiosis anthers, but is undetectable in
105 ear, embryo, or endosperm [19]. Microarray analysis of laser-microdissected anther cell
106 types [20,21] and *in situ* hybridization analysis of anther lobes [1,22] established that *Dcl5*
107 transcripts are highly enriched in the tapetum and are present at lower levels in pre-
108 meiotic pollen mother cells and meiocytes. RNA-seq confirmed *Dcl5* expression in
109 isolated maize meiocytes, however, quantitatively there are even higher levels in whole
110 anthers [23], as confirmed by newly-generated anther data (Supplementary Table 2).
111 Therefore, *Dcl5* is expressed much more highly in one or more somatic cell types than in
112 meiocytes [23]. Integrating prior observations that 24-nt phasiRNA biogenesis is contingent
113 on a normal tapetum [1], with the peak of *Dcl5* and DCL5 expression in meiotic anthers,
114 we conclude that the 24-nt phasiRNA pathway is localized in tapetal cells. We

115 hypothesize that this localization and timing is of functional importance for the
116 redifferentiation of tapetal cells into secretory cells during the meiotic period.
117

118 **24-nt phasiRNA abundance is greatly reduced in *dcl5* mutants**

119 To investigate if 24-nt phasiRNA biogenesis is affected in *dcl5* mutants, sRNA
120 libraries were constructed from anthers or spikelets of each *dcl5* allele (Supplementary
121 Table 2). Previously, we found that 24-nt phasiRNAs were readily detected from 176 24-
122 *PHAS* loci in W23 inbred anthers [1]. The 24-nt sRNAs produced from all these loci were
123 reduced dramatically in plants homozygous for each *dcl5* allele compared to fertile
124 siblings even though *dcl5-2* and *dcl5-3* encode proteins that lack only a few amino acids
125 (Fig. 3 and Supplementary Figure 5C). Other sRNAs, including 24-nt hc-siRNAs and 21-
126 nt phasiRNAs were retained (Supplementary Figure 11). We conclude that *Dcl5* is
127 required for 24-nt phasiRNA biogenesis and that the *dcl5-2* and *dcl5-3* mutations define
128 amino acids essential for DCL5 function. Analysis of *24-PHAS* precursors in RNA-seq
129 anther libraries from the same plants showed greater or nearly the same levels of
130 precursor abundance in each of the *dcl5* mutant alleles (Supplementary Figure 12).
131 Therefore, the absence of functional DCL5 severely disrupts processing of 24-nt
132 phasiRNA precursors with a modest impact on their accumulation.
133

134 Analysis of these RNA-seq data to characterize downstream transcriptional
135 pathways impacted in *dcl5* mutants was uninformative, consistent with prior results that
136 failed to identify mRNA targets for 24-nt phasiRNAs [1]. The transcriptional changes in
137 *dcl5-1* mutants were minimal (23 transcripts altered two-fold) and mainly corresponded

138 to genes expressed in later tapetal stages (Supplementary Table 3). Alterations in the
139 transcript population are likely indirect and reflective of defective tapetal development.
140

141 ***dcl5* mutants are temperature-sensitive male sterile**

142 During summer, 2016, *dcl5-1* field-grown plants exhibited variable fertility under
143 typical summer conditions in Stanford, CA: 25/18° C interrupted by multi-day heat
144 waves exceeding 32° C and short periods of cooler weather. To test whether temperature
145 is a restrictive condition, three controlled greenhouse regimes were chosen -- 28/22° C,
146 26/20° C, and 23/20° C (14 h day/10 h night temperature) -- and maintained within
147 narrow limits over the life cycle (Fig. 4 and Supplementary Figure 13). At 28/22° C,
148 *dcl5-1* mutants had shorter anthers that never exerted, while heterozygous siblings
149 developed normally. In contrast, under both the 26/20° C and 23/20° C regimes, *dcl5-1*
150 mutants were partially to fully fertile (see Methods for details of tassel development and
151 Supplementary Figure 13 for quantification of anther emergence); this conditional male
152 sterility was also observed in the transposon-disrupted *dcl5-mu03* allele (Supplementary
153 Figure 14). Under permissive conditions, *dcl5-1* pollen was viable based on Alexander
154 staining despite a prolonged life cycle and delayed flowering date under cooler
155 temperatures (Supplementary Figure 15); importantly, ears pollinated by such pollen
156 yielded viable progeny seed. At least one aspect of normal tapetal development was also
157 restored: the percentage of binucleated tapetal cells at 1.5 and 2.5 mm in *dcl5-1* anthers
158 was similar to their normal siblings (Supplementary Figure 16). In contrast, in comparing
159 *dcl5-1* transcript levels, 24-nt phasiRNA production, and *PHAS* precursor accumulation
160 in *dcl5-1* plants under restrictive and permissive temperatures, we observed no significant

161 differences; fertility-restored plants did not accumulate 24-nt phasiRNAs (Fig. 3,
162 Supplementary Figure 2 and Supplementary Figure 12). Our interpretation is that the
163 functions of *Dcl5* and 24-nt phasiRNAs are dispensable for tapetum development and
164 maize male fertility at low temperatures (23/20° C) but are required at higher
165 temperatures. Cool temperatures slow the pace of development and may allow alternative
166 pathways independent of the 24-nt phasiRNAs to support tapetal cell redifferentiation.
167
168 Maize tassels contain anthers representing seven days of development [24], and we
169 wondered if sporadic anther exertion in *dcl5-1* plants reflected a short phenocritical
170 period when some anthers experienced permissive conditions. Homozygous *dcl5-1* plants
171 were greenhouse-grown at 28/22° C until the tassel inflorescence formed (~30 days), then
172 plants were moved into two walk-in chambers: permissive 23/20° C or restrictive 28/22°
173 C regimes. In the next three weeks, 14 sets of three plants were swapped between the two
174 regimes for 3, 6, 9, 12, 15, 18 or 21 days, and then all plants finished their life cycle in
175 the 28/22° C greenhouse (Supplementary Figure 17). Plants in the 23/20° C regime from
176 the start of meiosis through the release of mononucleate microspores (~9 day period,
177 swaps 7 to 11, Supplementary Figure 17) were more fertile. Sample plants were assessed
178 during the 6th through 9th days to check anther staging in the main tassel spike,
179 confirming that this interval corresponds to meiosis and post-meiotic stages in the most
180 mature part of the tassel. These stages also encompass the initiation, peak, and continued
181 presence of 24-nt phasiRNAs in normal anthers [1]. Plants in the permissive temperature
182 for fewer than nine days during this interval had reduced fertility (swaps 1 to 6, 12 to 14);
183 we hypothesize that this extended interval is required to allow all anthers to proceed

184 through the phenocritical period to ensure full fertility. The temperature swap experiment
185 demonstrates that there is a short period in which DCL5 is required to "buffer"
186 development at elevated temperatures. Surprisingly, the restrictive temperature is similar
187 to what is considered optimal day temperature for the U.S. corn belt; historical data
188 indicate that growth between 20° to 29° C generates optimal yield, with higher yields
189 associated with warmer temperatures within this range [25,26].
190

191 **Discussion**

192 Maize DCL5 is essential for robust male fertility: *dcl5* plants are temperature-
193 sensitive during meiosis, show arrested tapetal development at this and later stages, and
194 lack 24-nt phasiRNAs. In rice, perturbed 21-nt, premeiotic phasiRNAs confer
195 photoperiod and temperature-sensitive male fertility [27-29]. Molecular and *in situ* analyses
196 in maize indicate that the 24-nt phasiRNA biogenesis factors and these sRNAs are
197 located primarily in the tapetum [1]. For maize, we conclude that 24-nt phasiRNAs play a
198 direct role in tapetal redifferentiation and only an indirect role in meiocytes or
199 gametophytes. We hypothesize that the 24-nt phasiRNAs are essential for tapetal
200 redifferentiation for biosynthesis and secretion of materials that support haploid
201 microgametophytes. The molecular mechanisms by which 21- and 24-nt reproductive
202 phasiRNAs act remain unclear, because they lack complementarity to mRNAs.
203

204 Conditional male sterility is common in rice. A number of loci regulating
205 photoperiod-sensitive genic male sterility (PMS) and thermo-sensitive genic male
206 sterility (TMS) have been mapped [27,28]. Two of these loci, *PMS1* and *PMS3*, encode long

207 non-coding RNAs [28,29]. *PMS1* is a *PHAS* locus that generates 21-nt phasiRNAs
208 associated with male fertility under long-day conditions [28]. *PMS3* also produces a small
209 RNA of 21-nt [29]. The rice *rna-dependent rna polymerase 6-1* (*rdr6-1*) mutant displays
210 various degrees of spikelet defects at high temperatures [5]. These findings suggest that
211 long non-coding RNAs and small RNAs are important regulators of male fertility
212 controlled by cross-talk between genetic pathways and environmental factors. Abiotic
213 stress-induced male sterility has been associated with alterations in tapetal development
214 in many plant species [30]. For example, *TMS10* and its close homolog *TMS10L* encode two
215 rice receptor-like kinases and are essential for tapetal degeneration and male fertility
216 under high temperatures [31].

217

218 In maize, conditional or partial male sterility has been reported, but not
219 extensively studied. The maize *ocl4-1* and *ocl4-2* mutants both show varying degrees of
220 male sterility, and the severity of the phenotype is strongly influenced by environmental
221 conditions [32]. OCL4 is a HD-ZIP IV transcription factor [32], and *ocl4* mutants lack 21-
222 phasiRNAs [1]. The OCL4 regulation of 21-nt phasiRNA biogenesis and the fact that male
223 sterility in the *dcl5* mutants is also sensitive to temperature indicate that the functions of
224 some secondary small RNAs support normal development and cellular functions during
225 environmental fluctuations outside the optimal temperature regime. The finding that *dcl5-*
226 *1* mutants are sterile under the 28/22° C regime suggests that 24-nt phasiRNA biogenesis
227 is essential for high corn yield under optimal U.S. summer farming conditions.

228

229 We can only speculate why the incredibly diverse and abundant 24-nt phasiRNAs
230 are required to support normal tapetal development under mild temperature stress. Plants
231 were well-watered under all growth conditions, and there were no obvious indicators of
232 water stress such as leaf rolling or leaf damage. Under warm temperatures, plant
233 development is accelerated relative to cooler conditions: the transition to flowering is
234 earlier and pollen shed is precocious. In the case of the temperature regimes we
235 employed, pollen shed was about 10 days earlier under the 28/22° C growth condition
236 than under cooler daytime temperatures (Fig. 4). It is possible that during more rapid
237 growth, there is a more stringent requirement for coordination of developmental
238 processes, requiring more rapid and complete switches from one developmental state to
239 another. Tapetal cells redifferentiate during meiosis, evidenced by accumulation of future
240 exine components and binucleate status. Because this is the only anther cell type with
241 obvious defects at peak 24-nt phasiRNA production at 2.0 mm, we hypothesize that the
242 abundant phasiRNAs are used to reset tapetal capabilities. Because 24-nt phasiRNAs lack
243 a high degree of complementarity to mRNAs other than their own precursors, one
244 hypothesis is that it is their sheer abundance that permits a resetting of development. For
245 example, the 24-nt phasiRNAs could bind to diverse AGO proteins, in effect displacing
246 miRNAs or other sRNAs involved in gene regulation associated with pre-meiotic tapetal
247 development. The 24-nt phasiRNAs could thus contribute to rapid redifferentiation of
248 tapetal cells during meiosis by eliminating gene expression regulation persisting from an
249 earlier developmental state. It is also possible that 24-nt phasiRNAs perform this or
250 another role in meiocytes or in other anther cell types, although their abundance is much
251 less than in non-tapetal cells. Alternatively, the functions of 24-nt phasiRNAs may

252 involve targeted action utilizing Argonautes or other RNA-binding proteins with as-yet
253 uncharacterized activities required in tapetal differentiation.
254
255 Our study in maize establishes that DCL5 plays a unique role, having
256 subfunctionalized from DCL3 for 24-nt phasiRNA biogenesis in anthers. *Dcl5* transcripts
257 are still expressed in diverse organs, however, protein and critical functions are restricted
258 to anthers. Expression analysis found just 23 genes differentially expressed in our *dcl5-1*
259 mutants, but all of these are likely reflective of arrested tapetal development. That the
260 thousands of 24-nt phasiRNAs fail to impact mRNA abundances significantly indicates
261 that 24-nt phasiRNAs are distinct from tasiRNAs which have specific mRNA targets and
262 modulate transcript abundances. DCL5 and therefore the 24-nt phasiRNAs are
263 dispensable at cool growing temperatures for maize, however, DCL5 is required for
264 robust fertility at temperatures for optimal yield in the U.S. corn belt. As climate
265 disruption, including more extensive heat waves, and a general warming trend increase
266 field temperatures, buffering maize tapetal development from adverse effects may be
267 possible by enhancing 24-nt phasiRNA functions. The 24-nt phasiRNAs may permit
268 development during other untested environmental challenges. Given the high degree of
269 variation typically observed across maize inbreds for many traits, the *dcl5* mutant
270 phenotype may also vary across inbreds. More generally, it is unknown how many crop
271 plants utilize reproductive phasiRNAs and whether their tapetal health and functions
272 could benefit by introduction or optimization of these or other sRNA pathways [30-32].
273
274 **Methods**

275 ***Dcl5* mutant generation and characterization**

276 To increase the CRISPR-based mutagenesis frequency in the targeted region, two
277 target sites separated by 76 bp were selected for guide RNA (gRNA) construction,
278 designed using the CRISPR Genome Analysis Tool [15]. Rice *U6* small nuclear RNA gene
279 promoters (P*U6.1* and P*U6.2*) were used to drive the expression of each gRNA. Two
280 guide RNAs (first gRNA, 5'-GTTCATGGTCTATCTGGAAAC-3'; second gRNA, 5'-
281 CTGGGTTCGTTCTCTTAA-3') were first selected; then two complementary
282 oligonucleotides for each guide RNA (g*ZmDcl5*-F1, 5'-
283 tgttGTTCATGGTCTATCTGGAAAC-3'; g*ZmDcl5*-R1, 5'-
284 aaacGTTTCCAGATAGACCATGAAC-3'; *gZmDcl5*-F3, 5'-
285 gtgtGCTGGGTTCGTTCTCTTAA-3'; g*ZmDcl5*-R3, 5'-
286 aaacTTAAGAGAACGAACCCAGC-3') were annealed to produce double-stranded
287 DNA oligos, then inserted into a pENTR based vector using *Btg*ZI and *Bsa*I (New
288 England BioLabs) restriction enzymes. These constructs were transferred using Gateway
289 recombination to the binary vector containing the *Cas9* gene driven by the maize
290 *Ubiquitin 1* promoter and the *bar* gene driven by *35S* promoter [15]. The final construct was
291 transformed into *Agrobacterium tumefaciens* for delivery into HiII maize immature
292 embryos, followed by screening of positive calli with T7E1 assay and Sanger sequencing
293 [15].

294

295 DNA samples were extracted from Basta®-resistant calli and screened for
296 mutations in the target region by PCR using primers *Dcl5*_F1 (5'-
297 ATCTAGATCTCCAGACCATTGAACCCTGTC-3') and *Dcl5*_R1 (5'-

298 GTATTCTAGACTTGAATAACCTGCTCTTTG-3'). Positive calli were transferred to
299 regeneration media; multiple plants regenerated from the same callus were considered to
300 be biological clones [15]. No chimeric plants were detected, consistent with Cas9 action in a
301 single cell. Leaves from mature T_0 plants were genotyped for a second time using PCR
302 amplification and Sanger sequencing to confirm the mutations. Over several generations
303 families were established that segregated 1:1 for *dcl5*//+ fertile: *dcl5//dcl5* homozygous
304 sterile individuals using standard maize genetic procedures.

305

306 *Mu* transposon population were first screened online (www.maizegdb.org and
307 teosinte.uoregon.org). Three candidates from Illumina-Mu population were identified
308 (*dcl5-mu01*, mu-illumina_252772.6; *dcl5-mu02*, mu-illumina_254833.6; *dcl5-mu03*, mu-
309 illumina_139042.7); one candidate from UniformMu was identified (*dcl5-mu04*, UFMu-
310 03512). The mutant information provided online showed the Mu insertions are expected
311 in either 5'-UTR region (*dcl5-mu02* and *dcl5-mu04*) or introns (*dcl5-mu01* and *dcl5-*
312 *mu03*), but we amplified the approximate region and found the third exon of *Dcl5* is
313 disrupted in *dcl5-mu03* with Sanger sequencing, using primer *Dcl5*-F2 (5'-
314 CATTAGTCAGGCAGTTGGTAGG-3') and *Dcl5*-R2 (5'-
315 GTGGCCCGTTTGTCTTCTCC-3'). Because the *Mu* transposon was in an exon, the
316 *dcl5-mu03* allele was the most promising candidate and pursued further. The
317 heterozygous plants were self-crossed to obtain a 3:1 segregating family, and
318 homozygous plants were identified by PCR and used for molecular and phenotypic
319 characterization.

320

321 **Microscopy and imaging**

322 For anther wall structure analysis with confocal microscopy, the anthers of
323 precisely measured sizes were dissected and stored in 70% ethanol for fixation. Fixed
324 anthers were then stained by propidium iodide and visualized on a Leica SP8 confocal
325 microscope [20]. Meiocytes were extruded and stained by DAPI (4',6-diamindino-2-
326 phenylindole) [33]. The Alexander's staining solution [34] was used to test the viability of the
327 pollen grains in the permissive conditions. For TEM [35], anthers were dissected and fixed
328 in fresh 0.1 M PIPES buffer (pH 6.8). A 2% osmium tetroxide stain was applied with
329 brief washes, followed by dehydration in an acetone gradient. Specimens were infiltrated
330 using a gradient of Spurr's resin (Sigma-Aldrich) and embedded. The sections were cut
331 using a Leica UCT ultramicrotome, stained in urayl and lead salts, and observed using a
332 Zeiss TEM instrument with a LEO 912 AB energy filter. Semi-thin sections were
333 obtained with the same method as TEM except for the heavy metal staining steps, and
334 imaged with Aperio Digital Pathology Slide Scanner with a 40x lens.

335

336 **ScaleP clearing of maize anthers**

337 Maize anthers were fixed directly into 4% paraformaldehyde in phosphate-
338 buffered saline (pH 7.4), and then prepared following the ScaleP protocol [36]. After 8 h
339 KOH treatment, anthers were stained for a week at room temperature with 1 mM
340 Calcofluor white for imaging of cell walls and 5 μM Syto13 (ThermoFisher) for imaging
341 nuclei. Samples were then cleared for three days with ScaleP solution consisting of 6 M
342 urea, 30% (v/v) glycerol, and 0.1% (v/v) Triton X-100 in sterile water. Cleared samples
343 were then imaged with a Zeiss 880 multi photon confocal microscope with a 40x LD C-

344 Apochromat water lens (numerical aperture of 1.1; working distance of 0.62 mm). The
345 3D rendering was performed with Amira (FEI, ThermoFisher) software. Tapetal cells
346 were classified as mononucleate or binucleate manually for the 2-D images, or
347 segmentated automatically for the 3-D images, and then artificially colored.

348

349 **sRNA-seq and RNA-seq library construction and sequencing**

350 Total RNA for sRNA-seq and RNA-seq libraries was isolated using the PureLink
351 Plant RNA Reagent (ThermoFisher). Total RNA quality was assessed by denaturing
352 agarose gel electrophoresis and quantified by the Qubit RNA BR Assay Kit
353 (ThermoFisher). For library preparation, 20 to 30 nt RNAs were excised from a 15%
354 polyacrylamide/urea gel, and ~25 ng of sRNA used for library construction with the
355 TruSeq Small RNA Prep Kit (Illumina); alternatively, RealSeq®-AC kits (SomaGenics)
356 were used for ultra-low amount of total RNA starting from 100 ng. For RNA-seq, 2 μg of
357 total RNA was treated with DNase I (New England BioLabs) and then cleaned with RNA
358 Clean and Concentrator-5 (Zymo Research). The TruSeq Stranded Total RNA with
359 RiboZero-Plant Kit (Illumina) or NEBNext Ultra II Directional RNA Library Prep Kit
360 (New England BioLabs) was used for library construction with 500 ng of treated RNA.
361 Sequencing in single-end mode on an Illumina HiSeq 2500 or NextSeq (University of
362 Delaware) yielded 51 or 75 bp reads for both sRNA-seq and RNA-seq.

363

364 For sRNA-seq data [37], we first used Trimmomatic version 0.32 to remove the
365 linker adaptor sequences [38]. The trimmed reads were then mapped to version 4 of the B73

366 maize genome using Bowtie [39]. Read counts were normalized to 20 million to allow for
367 the direct comparison across libraries. phasiRNAs were designated based on a 24-nt
368 length and mapping coordinates within the previously identified 176 *24-PHAS* loci [1],
369 updated to version 4 of the B73 genome using the assembly converter tool [40]. If a 24-nt
370 phasiRNA did not uniquely map to the genome, we divided the abundance equally to
371 each location to which the read mapped, i.e. a hits-normalized abundance. These hits-
372 normalized abundances were then summed for each of the 176 loci to calculate the 24-nt
373 phasiRNA abundances.

374

375 RNA-seq libraries were trimmed as above, and mapped to version 4 of the B73
376 genome using Tophat version 2.0.12 [41]. For differential expression analysis of genes, we
377 assembled the transcripts using the Cufflinks package [42] and raw gene expression levels
378 were quantified using FeatureCounts version 1.5.0 [43] to generate count tables that were
379 imported into R for statistical analysis [44]. Weakly expressed transcripts (fewer than 1
380 read) were filtered out, and the remaining transcripts were normalized using DEseq2 to
381 identify a set of differentially expressed genes for anthers homozygous for each mutant
382 allele [45]. Due to a lack of a replicate for the *dcl5-1* restrictive library, we calculated
383 dispersions using the mean of libraries to identify differentially expressed transcripts
384 without a complete set of replicates.

385

386 For differential expression analysis of the *PHAS* precursors, we were unable to
387 assemble the transcripts that mapped to these regions because of the absence of
388 annotation in any feature files. Instead, we conducted this analysis in parallel to the

389 analysis of the sRNA data. We first normalized the mapped fragmented reads as counts
390 per 15 million, and applied the hits-normalized abundance approach described above.
391 Using the annotated *24-PHAS* loci (above), we then identified the summed abundance of
392 RNA-seq transcript fragments that mapped to these regions to identify a representative
393 abundance for each *24-PHAS* precursor. Replicate libraries were averaged together prior
394 to the construction of the heatmap, and we added 1 to all abundances in order to prevent
395 $\log_2(0)$ error while also giving the added benefit of removing negative log transformed
396 values. Boxplots were generated for each replicate's log transformed values.

397

398 **Determination of male fertility**

399 Anther exertion on male fertile tassel take approximately seven days: Anthers
400 emerge from the upper florets of the center of main spike on day 1; day 2 will include
401 anthers from the lower florets in the center of the main spike and additional upper florets
402 from the main spike (above and below the middle zone); day 3 will include lower floret
403 spikes from the zones that stated on day 2, plus the upper florets at the base of the main
404 spike and the middle of the primary branches; day 4 will include lower florets from the
405 spikelets involved on day 3, plus upper florets from more regions on the primary
406 branches; day 5 will include the lower florets from spikelets involved on day 4; day 6 will
407 include the upper florets on the secondary branches, and day 7 will include the lower
408 florets of the secondary branches [24]. Based on the maize anther emergence, tassel at
409 similar stages in anther emergence were chosen for photographs and quantification.

410

411 Tassel RGB images were obtained with cell phones with digital cameras. Then, a
412 quantitative image-based color trait analysis pipeline on the PlantCV V2 [46,47] platform
413 (https://plantcv.danforthcenter.org) was applied to determine the male fertility, with a
414 computational segmentation algorithm. In brief, the naïve Bayes approach was applied
415 and three classes (anther; other tassel parts; and background) of labeled pixels were used
416 to segment tassel images. By using these three classifiers, anthers and other parts of tassel
417 were highlighted in red and green. Then, area of anther and tassel from each tassel was
418 summed and used to calculate anther/tassel area ratio, as an indicator for male fertility.
419

420 **Data Availability**

421 Requests for materials should be addressed to walbot@stanford.edu. Raw data were
422 submitted to GEO under GSE122449
423 [https://www.ncbi.nlm.nih.gov/geo/query/acc.cgi?acc=GSE122449] (including sRNA-
424 seq as GSM3466686 to GSM3466700 and GSM4180400 to GSM4180404; and RNA-seq
425 data as GSM3466701 to GSM3466714, and GSM4180405 to GSM4180408), and the
426 processed data are available via our maize genome browser at
427 https://mpss.danforthcenter.org. Other supporting data are available from the
428 corresponding authors upon request.

429 **References**

430 1. Zhai, J. *et al.* Spatiotemporally dynamic, cell-type–dependent premeiotic and meiotic
431 phasiRNAs in maize anthers. *Proc. Natl. Acad. Sci.* ***112*****,** 3146–3151 (2015).
432 2. Xia, R. *et al.* 24-nt reproductive phasiRNAs are broadly present in angiosperms. *Nat.*
433 *Commun.* ***10,*** 627 (2019).
434 3. Johnson, C. *et al.* Clusters and superclusters of phased small RNAs in the developing
435 inflorescence of rice. *Genome Res.* ***19*****,** 1429–1440 (2009).
436 4. Song, X. *et al.* Roles of DCL4 and DCL3b in rice phased small RNA biogenesis.
437 *Plant J.* ***69*****,** 462–474 (2012).
438 5. Song, X. *et al.* Rice RNA-dependent RNA polymerase 6 acts in small RNA
439 biogenesis and spikelet development. *Plant J.* ***71*****,** 378–389 (2012).
440 6. Nonomura, K.-I. *et al.* A germ cell specific gene of the *ARGONAUTE* family is
441 essential for the progression of premeiotic mitosis and meiosis during sporogenesis in
442 rice. *Plant Cell* ***19*****,** 2583–94 (2007).
443 7. Komiya, R. *et al.* Rice germline-specific Argonaute MEL1 protein binds to
444 phasiRNAs generated from more than 700 lincRNAs. *Plant J.* ***78*****,** 385–397 (2014).
445 8. Nonomura, K.-I. Small RNA pathways responsible for non-cell-autonomous
446 regulation of plant reproduction. *Plant Reprod.* ***31*****,** 21–29 (2018).
447 9. Ono, S. *et al.* EAT1 transcription factor, a non-cell-autonomous regulator of pollen
448 production, activates meiotic small RNA biogenesis in rice anther tapetum. *PLOS*
449 *Genet.* ***14,*** e1007238 (2018).
450 10. Margis, R. *et al.* The evolution and diversification of Dicers in plants. *FEBS Lett.*
451 ***580*****,** 2442–2450 (2006).

452 11. Thompson, B. E. *et al.* The *dicer-like1* homolog *fuzzy tassel* is required for the
453 regulation of meristem determinacy in the inflorescence and vegetative growth in
454 maize. *Plant Cell* ***26*****,** 4702–4717 (2014).
455 12. Parent, J. S., Bouteiller, N., Elmayan, T. & Vaucheret, H. Respective contributions of
456 Arabidopsis DCL2 and DCL4 to RNA silencing. *Plant J.* ***81*****,** 223–232 (2015).
457 13. Daxinger, L. *et al.* A stepwise pathway for biogenesis of 24-nt secondary siRNAs and
458 spreading of DNA methylation. *EMBO J.* ***28*****,** 48–57 (2009).
459 14. Gasciolli, V., Mallory, A. C., Bartel, D. P. & Vaucheret, H. Partially redundant
460 functions of Arabidopsis DICER-like enzymes and a role for DCL4 in producing
461 trans-acting siRNAs. *Curr. Biol.* ***15*****,** 1494–1500 (2005).
462 15. Char, S. N. *et al.* An Agrobacterium-delivered CRISPR/Cas9 system for high-
463 frequency targeted mutagenesis in maize. *Plant Biotechnol. J.* ***15*****,** 257–268 (2017).
464 16. Williams-Carrier, R. *et al.* Use of Illumina sequencing to identify transposon
465 insertions underlying mutant phenotypes in high-copy *Mutator* lines of maize. *Plant*
466 *J.* ***63,*** 167-177 (2010).
467 17. Sekhon, R. S. *et al.* Genome-wide atlas of transcription during maize development.
468 *Plant J.* ***66*****,** 553–563 (2011).
469 18. Stelpflug, S. C. *et al.* An expanded maize gene expression atlas based on RNA
470 sequencing and its use to explore root development. *Plant Genome* ***9*** (2016).
471 19. Walley, J. W. *et al.* Integration of omic networks in a developmental atlas of maize.
472 *Science* ***353*****,** 814–818 (2016).
473 20. Zhang, H. *et al.* Transcriptomes and proteomes define gene expression progression in
474 pre-meiotic maize anthers. *G3* ***4*****,** 993–1010 (2014).

475 21. Kelliher, T. & Walbot, V. Maize germinal cell initials accommodate hypoxia and
476 precociously express meiotic genes. *Plant J.* ***77*****,** 639–652 (2014).
477 22. Nan, G.-L. *et al.* MS23, a master basic helix-loop-helix factor, regulates the
478 specification and development of tapetum in maize. *Development* ***144*****,** 163–172
479 (2017).
480 23. Dukowic-Schulze, S. *et al.* Novel meiotic miRNAs and indications for a role of
481 phasiRNAs in meiosis. *Front. Plant Sci.* ***7*****,** 762 (2016).
482 24. Egger, R. L. & Walbot, V. Quantifying *Zea mays* L tassel development and
483 correlation with anther developmental stages as a guide for experimental studies.
484 *Maydica* ***60*****,** (2015).
485 25. Schlenker, W. & Roberts, M. J. Nonlinear effects of weather on corn yields. *Rev.*
486 *Agric. Econ.* ***28*****,** 391–398 (2006).
487 26. Schlenker, W. & Roberts, M. J. Nonlinear temperature effects indicate severe
488 damages to U.S. crop yields under climate change. *Proc. Natl. Acad. Sci.* ***106*****,**
489 15594–15598 (2009).
490 27. Zhou, H. *et al.* Photoperiod- and thermo-sensitive genic male sterility in rice are
491 caused by a point mutation in a novel noncoding RNA that produces a small RNA.
492 *Cell Res.* ***22*****,** 649–660 (2012).
493 28. Fan, Y. *et al.* PMS1T, producing phased small-interfering RNAs, regulates
494 photoperiod-sensitive male sterility in rice. *Proc. Natl. Acad. Sci.* ***113*****,** 15144–15149
495 (2016).
496 29. Ding, J. *et al.* A long noncoding RNA regulates photoperiod-sensitive male sterility,
497 an essential component of hybrid rice. *Proc. Natl. Acad. Sci.* ***109*****,** 2654–2659 (2012).

498 30. Storme, N. D. & Geelen, D. The impact of environmental stress on male reproductive
499 development in plants: biological processes and molecular mechanisms. *Plant Cell*
500 *Environ.* ***37*****,** 1–18 (2014).
501 31. Yu, J. *et al.* Two rice receptor-like kinases maintain male fertility under changing
502 temperatures. *Proc. Natl. Acad. Sci.* ***114***, 12327-12332 (2017).
503 32. Vernoud, V. *et al.* The HD-ZIP IV transcription factor OCL4 is necessary for
504 trichome patterning and anther development in maize. *Plant J.* ***59*****,** 883–894 (2009).
505 33. Zhang, H. *et al.* Stable integration of an engineered megabase repeat array into the
506 maize genome. *Plant J.* ***70*****,** 357–365 (2012).
507 34. Alexander, M. P. Differential staining of aborted and nonaborted pollen. *Biotech.*
508 *Histochem.* ***44*****,** 117–122 (1969).
509 35. Wang, L. *et al.* Characterization and fine mapping of a necrotic leaf mutant in maize
510 (*Zea mays* L.). *J. Genet. Genomics* ***40*****,** 307–314 (2013).
511 36. Warner, C. A. *et al.* An optical clearing technique for plant tissues allowing deep
512 imaging and compatible with fluorescence microscopy. *Plant Physiol.* ***166*****,** 1684–
513 1687 (2014).
514 37. Mathioni, S. M., Kakrana, A. & Meyers, B. C. Characterization of plant small RNAs
515 by next generation sequencing. *Curr. Protoc. Plant Biol* ***2*****,** 39–63 (2017).
516 38. Bolger, A. M., Lohse, M. & Usadel, B. Trimmomatic: A flexible trimmer for
517 Illumina sequence data. *Bioinformatics* ***30*****,** 2114–2120 (2014).
518 39. Kersey, P. J. *et al.* Ensembl Genomes 2016: more genomes, more complexity. *Nucl.*
519 *Acids Res.* ***44*****,** D574–D580 (2016).

520 40. Tello-Ruiz, M. K. *et al.* Gramene 2018: Unifying comparative genomics and pathway
521 resources for plant research. *Nucl. Acids Res.* ***46*****,** D1181–D1189 (2018).
522 41. Trapnell, C., Pachter, L. & Salzberg, S. L. TopHat: Discovering splice junctions with
523 RNA-Seq. *Bioinformatics* ***25*****,** 1105–1111 (2009).
524 42. Trapnell, C. *et al.* Transcript assembly and quantification by RNA-Seq reveals
525 unannotated transcripts and isoform switching during cell differentiation. *Nat.*
526 *Biotechnol.* ***28*****,** 511–515 (2010).
527 43. Liao, Y., Smyth, G. K. & Shi, W. FeatureCounts: An efficient general purpose
528 program for assigning sequence reads to genomic features. *Bioinformatics* ***30*****,** 923–
529 930 (2014).
530 44. R Development Core Team. *R: A language and environment for statistical*
531 *computing. R Foundation for Statistical Computing* ***1*** (2011).
532 45. Love, M. I., Huber, W. & Anders, S. Moderated estimation of fold change and
533 dispersion for RNA-seq data with DESeq2. *Genome Biol.* ***15*****,** 550 (2014).
534 46. Fahlgren, N. *et al*. A versatile phenotyping system and analytics platform reveals
535 diverse temporal responses to water availability in Setaria. *Mol. Plant* ***8***, 1520-1535
536 (2015).
537 47. Gehan, M. A. *et al*. PlantCV v2: Image analysis software for high-throughput plant
538 phenotyping. *Peerj* ***5***, e4088 (2017).
539

540 **Acknowledgments**

541 The *dcl5* CRISPR mutants were generously generated by Si Nian Char in Dr.
542 Bing Yang's group at Iowa State University (now University of Missouri – Columbia)

543 and were key to initiating the overall study. The *dcl5-mu03* allele was provided by Dr.
544 Alice Barkan at the University of Oregon. TEM images were produced and imaged by
545 Dr. Howard Berg at the Donald Danforth Plant Science Center. Semi-thin section images
546 were produced with the help of Shannon Modla in the BioImaging Center at the
547 University of Delaware. We thank the greenhouse staff at the Donald Danforth Plant
548 Science Center for facilitating the temperature swap experiment, Sandra Mathioni for the
549 preparation of small RNA and RNA-seq libraries, and Jeff Caplan for advice on
550 microscopy. **Funding:** This work was supported by U.S. National Science Foundation
551 Plant Genome Research Program (NSF-PGRP) awards 1649424 and 1754097. Author
552 contributions: H.Z., B.C.M, and V.W. conceived of the project, H.Z., C.T., and K.H.
553 performed and interpreted experiments, R.Z. analyzed sequencing data, H.Z. and C.T.
554 wrote the manuscript with editing by V.W., B.C.M, and with input from all co-authors.

555

556 **Competing Interests:** The authors declare no competing interests.

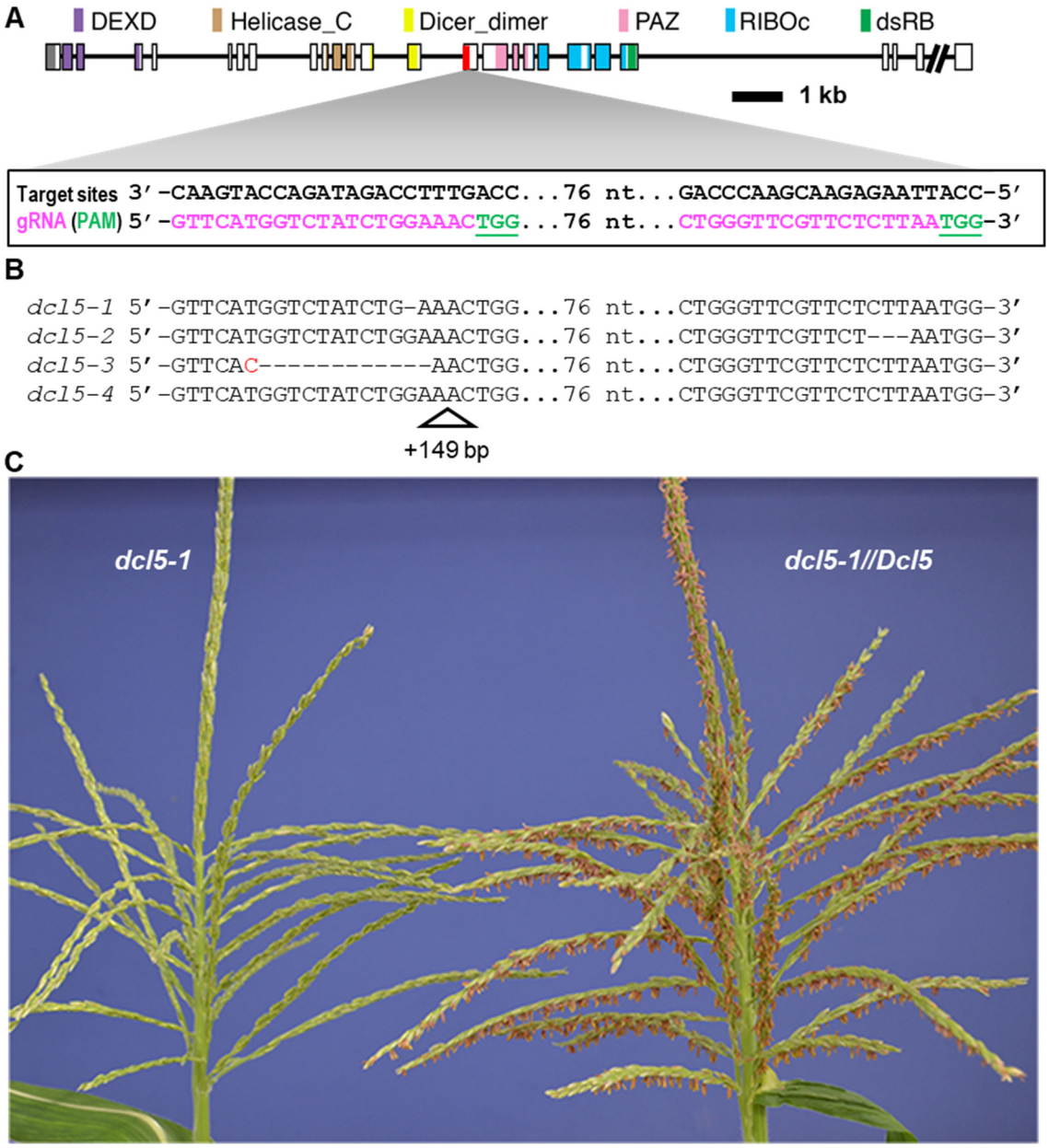

Fig. 1. CRISPR-Cas9 was used in maize to mutate *Dcl5*.
(A) Schematic diagram of the *Dcl5* gene model. Conserved domains were identified using the NCBI conserved domain search tool against database CDD v3.16. All domains were found with extremely high confidence except the double stranded RNA-binding (dsRB) domain, which had an e-value of 0.05. (**B)** Sequences of the four CRISPR-Cas9-generated mutant alleles selected for this study. (**C)** A *dcl5-1* tassel lacking any exerted anthers (left) and a sibling heterozygous *dcl5-1//Dcl5* plant at peak pollen shed with hundreds of exerted anthers (right).

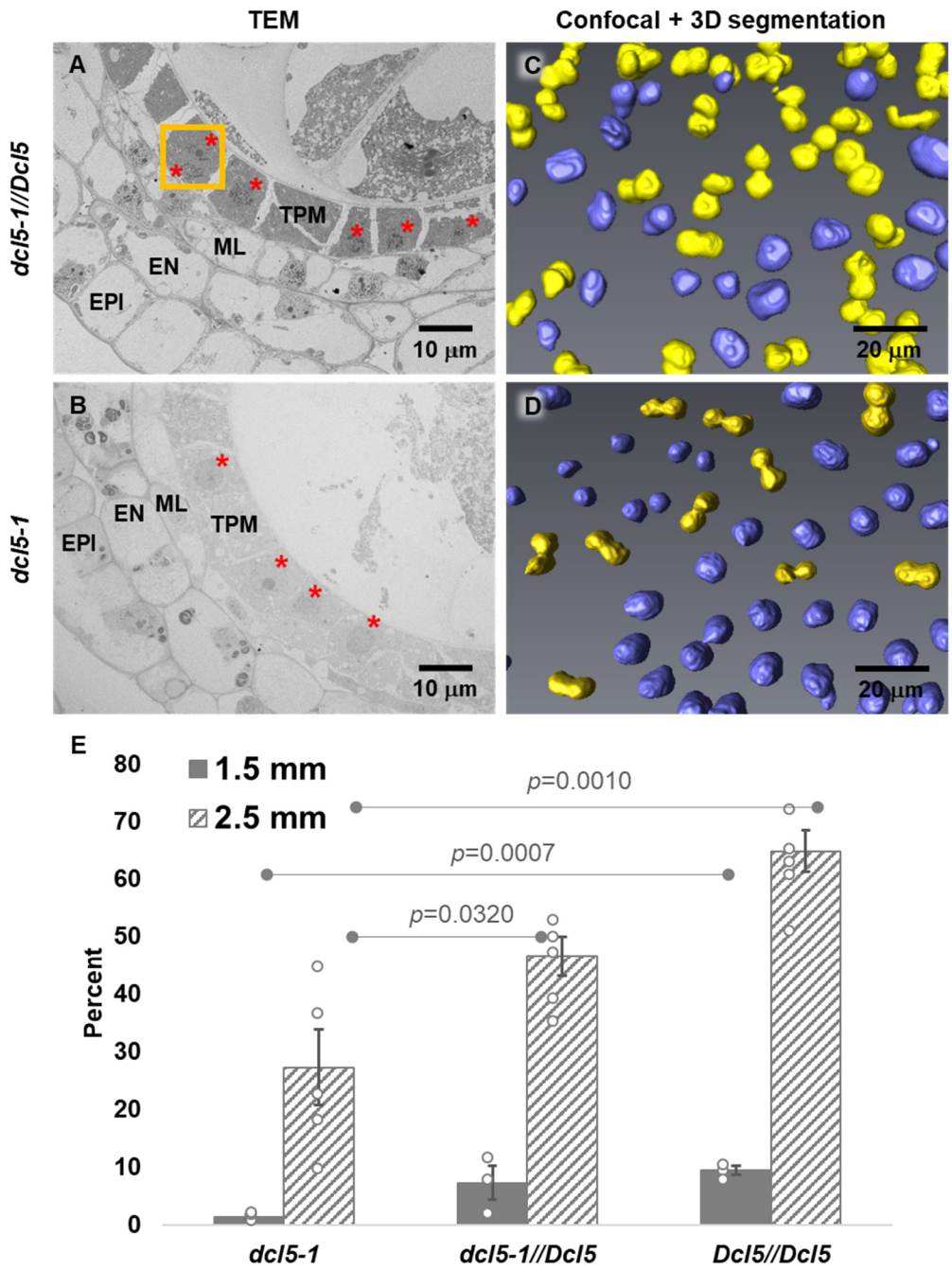

Fig. 2. Tapetal cells in *dcl5-1* plants are delayed or arrested in achieving binucleate status.

(A) Transmission electron microscopy (TEM) of a fertile *dcl5-1//Dcl5* 2 mm anther lobe. At this stage, the tapetal cells (TPM) are packed with dark staining materials, likely exine components later secreted onto haploid microspores. The middle layer (ML), endothecial (EN), and epidermal (EPI) cells are highly vacuolated. The orange boxes mark two binucleated tapetal cells in which both nuclei were visible (red dots). **(B)** TEM of a sterile *dcl5-1* anther lobe at the same stage, demonstrating distended, pale-staining, and mononucleate tapetal cells. Two anthers as replicates from *dcl5-1//Dcl5* and two anthers

from *dcl5-1* were used for TEM study. The other replicate is shown in Supplementary Figure 8. **(C)** *dcl5-1//Dcl5*, and **(D)** *dcl5-1:* three-dimensional reconstructions of cleared, 2.5 mm anthers stained with the nuclear marker Syto13. Individual nuclei of mononucleate tapetal cells are marked in purple, and binucleated cells are marked in yellow. **(E)** Quantification of binucleated cells in *dcl5-1*, *dcl5-1//Dcl5,* and *Dcl5//Dcl5* siblings at the meiotic I (1.5 mm) and meiotic II (2.5 mm) stages, in a family segregating 1:2:1. Statistics: two-tailed Student's T test. Three replicates were used for 1.5 mm anthers of each genotype; five replicates were used for 2.5 mm anthers of each genotype. Grey dots represent individual replicates (see Source Data File).

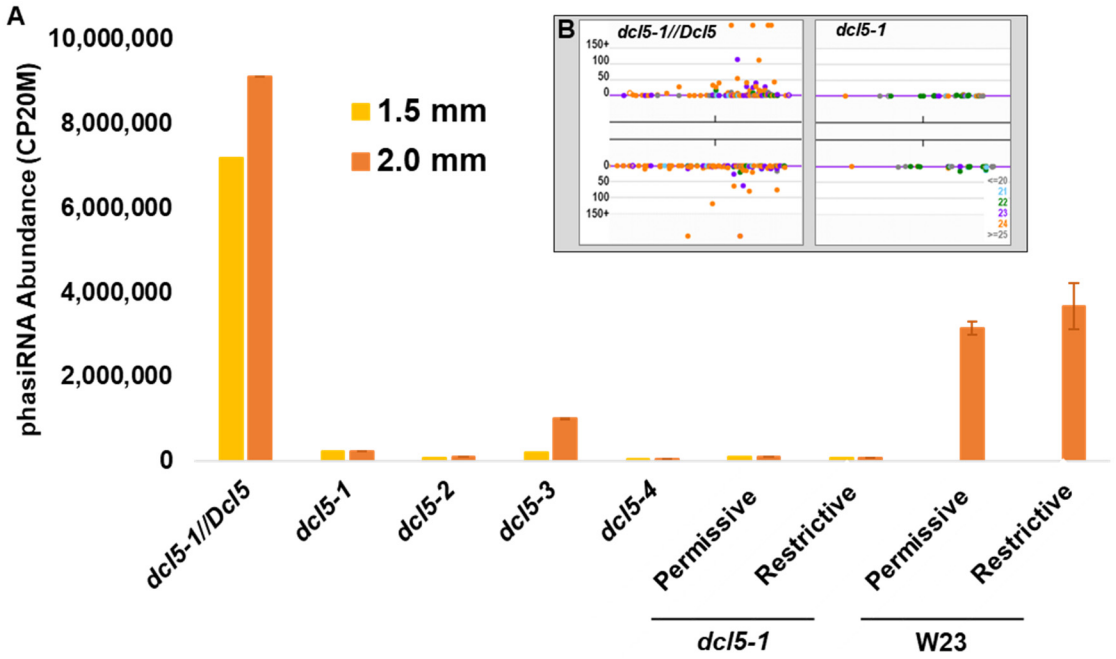

Fig. 3. Near absence of 24-nt phasiRNAs in CRISPR-derived *dcl5* mutant alleles. **(A)** Total 24-nt phasiRNAs from 176 *24-PHAS* loci are highly abundant in both 1.5 and 2.0 mm fertile heterozygous anthers, but abundance is reduced by >99% in *dcl5-1, dcl5-2,* and *dcl5-4*, and by >90% in *dcl5-3* anthers. Altered temperature regimes do not restore 24-nt phasiRNA abundances in either fertile (permissive) or sterile (restrictive) *dcl5-1* anthers (see main text). W23 inbred fertile anthers have similar 24-nt phasiRNA abundance under both temperature regimes. **(B, inset)** Representative *24-PHAS* locus #12 (B73, v4; chr 1, 178454619 bp) in a genome browser showing ~1.5 kbp with sRNAs in the fertile heterozygote (left) and *dcl5-1* (right). Orange dots are individual 24-nt phasiRNAs; x-axis is genome position on the top or bottom strand, and the y-axis depicts abundance in each genotype. Other colored dots are as indicated in the key, lower right.

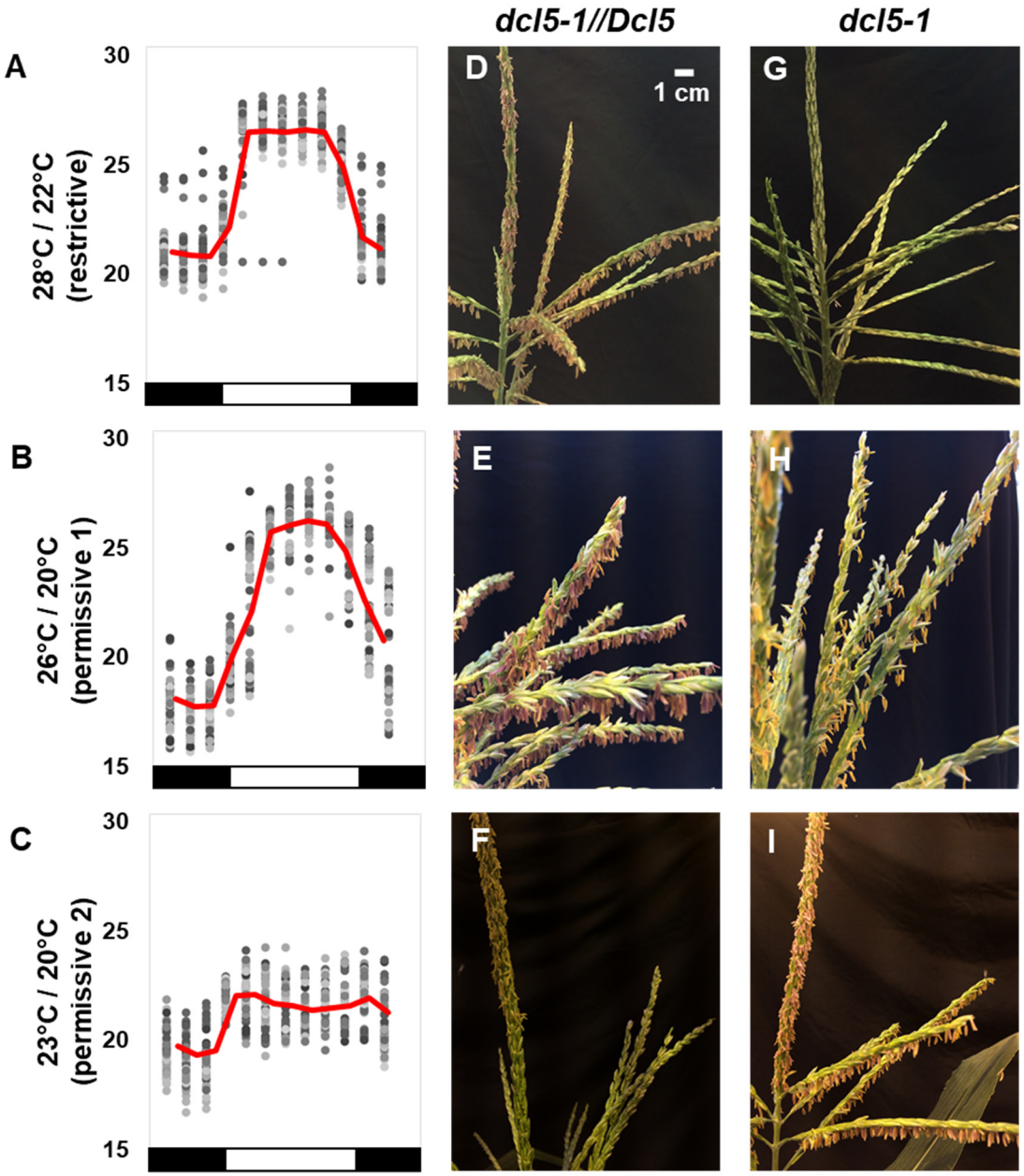

Fig. 4. *dcl5-1* anther fertility is temperature sensitive.
Three sets of *dcl5-1* and sibling *dcl5-1//Dcl5* plants grown in greenhouses with differing temperature regimes: 28°/22° C, 26°/20° C, or 23°/20° C (day/night). **(A, B, C)** Temperatures were recorded every 2 h for 60 days (grey dots, average in red; day/night indicated as white or black, below). **(D, E, F)** Heterozygous *dcl5-1//Dcl5* siblings were fully fertile under all three regimes. **(G, H, I)** *dcl5-1* plants in the restrictive regime **(G)** were completely male sterile, while those in permissive conditions were partially **(H)** or fully **(I)** fertile. Images were taken at 60±3 days after planting (DAP) (top row), 70±2 DAP (middle row), and 71±3 DAP (bottom row); the pace of tassel development is temperature-dependent and full anther exertion occurs at different days after planting, for example **(F)** was photographed on the first day of anther exertion, a seven-day process (See Methods). The scale bar in **(D)** is approximate and pertains to all tassel images.

Inventory of Supplementary Materials:

Supplementary Figures 1-17

Supplementary Tables 1-3